Electronic Supplementary Material (ESI) for Sustainable Energy & Fuels.

Selective oxidation of 5-hydroxymethylfurfural to 2, 5-diformylfuran with $ZnIn_2S_4$ 2D nanosheets and atmospheric O_2 under visible light

Shuoping Ding[a], José Balena Gabriel Filho[a], Tim Peppel[a], Simon Haida[a], Jabor Rabeah[a], Norbert Steinfeldt*[a], Jennifer Strunk*[ab]

[a]*Leibniz-Institut für Katalyse e. V. (LIKAT), Albert-Einstein-Str. 29a, 18059 Rostock, Germany*

[b]*Technische Universität München, School of Natural Sciences, Lichtenbergstr. 4, 85748 Garching, Germany.*

*Corresponding author

E-mail: Norbert.Steinfeldt@catalysis.de (Norbert Steinfeldt), Jennifer.Strunk@catalysis.de (Jennifer Strunk)

Experimental

Chemicals

5-Hydroxymethylfurfural (HMF, >99%), 2, 5-diformylfuran (DFF), and 2-formyl-5-furancarboxylic acid (FFCA) were purchased from endothermic life science molecules. Benzyl alcohol (>99%, Acros Organics) and benzaldehyde (>99.5%, Acros Organics) were utilized for benzyl alcohol oxidation experiment. 4-Chloro-2-nitrophenol (CN, >97%, Sigma Aldrich), p-benzoquinone ($C_6H_4O_2$, >98%, Sigma Aldrich), isopropanol (C_3H_8O, 99.9%, Sigma Aldrich), $K_2S_2O_8$ (≥99.0%, Sigma Aldrich), ethylenediaminetetraacetate (EDTA, Sigma Aldrich) were used for scavenger experiment. 5, 5-Dimethyl-1-pyrroline N-oxide (DMPO, Biotechnik GERBU) and 2, 2, 6, 6-Tetramethyl-piperidin (TEMP, Sigma Aldrich) were applied in EPR measurement. Zinc acetate dehydrate (Zn $(CH_3COO)_2 \cdot 2H_2O$, ≥99.5%, Merck), Indium nitrate ($In(NO_3)_3 \cdot XH_2O$, Chempur), Thioacetamide (TAA, ≥99.0%, Glentham Life Sciences Ltd), and ethanol (CH_3CH_2OH, ≥ 99.8%, Fisher Chemical), and trisodium citrate dehydrate ($Na_3C_6H_5O_7 \cdot 2H_2O$, ≥99%, Fisher Chemical) were used to synthesize materials. Reagents were analytical grade and directly used without further purification. Deionized water was used throughout all experiment. All chemicals were used as received without further purification.

Synthesis of $ZnIn_2S_4$ nanosheets

Zn $(CH_3COO)_2 \cdot 2H_2O$ (2.0 mmol, 0.439g), In $(NO_3)_3 \cdot XH_2O$ (4.0 mmol, 1.203g), TAA (3.2 mmol, 1.202g), and different amount of $Na_3C_6H_5O_7 \cdot 2H_2O$ (2mmol, 0.6g, 4mmol, 1.2g) were dissolved in 150 mL of H_2O and stirring for 30 minutes. Then the mixed solution was transferred into a 250 mL Teflon-lined stainless-steel autoclave and maintained at 180 °C for 24 h. After reaction, the products were collected by centrifuged at 8000 rpm and washed with water and ethanol several times. Finally, the photocatalysts were dried at 80 C overnight.

Synthesis of $ZnIn_2S_4$ without trisodium citrate, ZnS and In_2S_3

$Zn(CH_3COO)_2 \cdot 2H_2O$ (2.0 mmol, 0.439g), In $(NO_3)_3 \cdot XH_2O$ (4.0 mmol, 1.203g), and TAA (3.2 mmol, 1.202g) were dissolved in 75 mL H_2O and 75mL CH_3CH_2OH and stirring for 30 minutes. Then the mixed solution was

transferred into a 250 mL Teflon-lined stainless-steel autoclave and maintained at 180 °C for 24 h. After reaction, the photocatalysts were collected by centrifuged at 8000 rpm min^{-1} and washed with water and ethanol several times. Finally, the photocatalysts were dried at 80 C for overnight. ZnS was synthesized as the same procedure without addition of $In(NO_3)_3 \cdot XH_2O$. In_2S_3 was synthesized with the molar ratio of into TAA at 2: 3 (molar ratio of In to TAA was 6).

Characterization

X-ray diffraction (XRD) powder patterns were recorded on a Panalytical X'Pert diffractometer equipped with a linear position sensitive detector (PSD) using automatic divergence slits and Cu Kα1 radiation (40 kV, 40 mA, λ = 1.5406 Å).

X-ray photoelectron spectroscopy (XPS) measurements were performed in VG ESCALAB220iXL (Thermo Fisher Scientific, USA) with a monochromated Al Kα X-ray radiation source (E= 1486.6 eV).

Brunauer-Emmett-Teller (BET) surface area and porosity were obtained by the N_2 adsorption-desorption isotherms on an ASAP 2020 Micromeritics instrument. All samples were degassed at 100 °C for 3 h to desorb moisture and impurities from their surfaces. The pore size distributions were calculated using the Barrett-Joyner-Halenda (BJH) model from the desorption branch.

UV-vis diffuse reflectance spectra (DRS) were recorded on a AvaSpec 2048 fiber optical spectrometer (Avantes BV, Apeldoorn, Netherlands) equipped with an Ava Light-DHS light source and an FCR-19UV200-2-ME reflection probe by using $BaSO_4$ as the reference standard material.

Raman spectra were obtained on a inVia Raman microscope (Renishaw, Germany) by loading the material into a sample holder under ambient conditions. The excitation wavelength was 442 nm at a laser power of 5.8 mW.

The morphology and microstructure were observed on a field emission scanning electron microscope (FE-SEM, MERLIN® VP Compact, Co. Zeiss, Oberkochen) and a transmission electron microscope (TEM, JEM-ARM200F, JEOL) operating at an accelerated voltage of 200 kV. The sample was ultrasonically dispersed in ethanol solution, and a drop was deposited on a copper grid covered with a holey carbon membrane for observation.

Electron paramagnetic resonance (EPR) spectra were recorded on an X-band microwave spectrometer (EMX CW, Bruker Biospin GmbH, Rheinstetten, Germany) with a microwave frequency of about 9.7 GHz at room temperature.

X-ray photoelectron spectroscopy (XPS) measurements were performed in VG ESCALAB220iXL (Thermo Fisher Scientific, USA) with a monochromated Al Kα X-ray radiation source (E= 1486.6 eV).

Photocatalytic HMF oxidation experiment

In a typical experiment, the photocatalytic oxidation of HMF was carried out in a homemade photoreactor. 10 mg of sample was dispersed in 2 mL HMF (concentration: 20 mM) of CH_3CN solution under synthetic Air flowing at 15 °C. The reactor was illuminated with blue LED lamp (maximum wavelength: 467nm) with a light intensity of 25 mW•cm^{-2} (Fig. S1). At each 2 h, 50 μL of aliquot of the catalytic reaction solution was collected, diluted twenty times with water to 1 mL and analyzed with a high-performance liquid chromatography (HPLC, Agilent 1260) equipped with a 300 mm organic acid resin column with 7.80 mm inner diameter (Rezex ROA-Organic Acid, 00H-0138-K). 2 mM trifluoroacetic acid (TFA) aqueous solution (149 μL TFA was dissolved in 1L H_2O) was used as the mobile phase with a flow rate of 0.6 mL min^{-1} at a temperature of 40°C, and the injection volume was 10μL. The furan compounds were detected by a diode array detector (DAD) at 270 nm, and the retention times of FDCA, FFCA, HMFCA, HMF and DFF (HMF and all possible oxidation products, Fig. S2) were around 12.2, 16.8, and 21.6, 36.7, 45.8 min, respectively (Fig. S3). The concentration of furan compounds (FFCA, HMF and DFF) was quantified according to the external standard calibration curves (Fig. S4).

The HMF conversion, and selectivity and the yield of DFF were calculated using Equations (1), (2) and (3):

$$Conversion(\%) = \frac{C_{HMF\ initial} - C_{HMF\ after\ reaction}}{C_{HMF\ initial}} \times 100\% \#(1)$$

$$Selectivity(\%) = \frac{C_{DFF\ after\ reaction}}{C_{HMF\ initial} - C_{HMF\ after\ reaction}} \times 100\% \#(2)$$

$$Yield(\%) = \frac{C_{DFF\ after\ reaction}}{C_{HMF\ initial}} \times 100\% \#(3)$$

H_2O_2 measurement

The hydrogen peroxide concentration was determined by the titanium complex colorimetric method [1, 2]. Briefly, 1 mL of the sample was added to 3 mL of acidified solution of ammonium titanyl oxalate monohydrate (8.33 g/L) , the color of the solution turned yellow and maintained for 30s.The absorbance of the peroxo complex formed by the reaction between Ti(IV) and the hydrogen peroxide was measured at 400 nm using an Avantes UV-Vis spectrophotometer model AvaSpec-2048 (equipped with a Ava Light-DH-S-BAL light source and 0.5 cm optical pathway glass fiber probe) and the quantification was made by a linear calibration curve ranging from 0.3 to 4 mM.

DMPO and TEMP measurements

For the tests, a suspension was made in a 2 mL vial by weighing 5 mg of the photocatalyst and adding it to a solution with 100 mM of spin trapping molecule (DMPO to capture radical species and TEMP for $^1O_2$) in acetonitrile, which was previously saturated with oxygen. This suspension was then irradiated by a blue LED, stirred, and aliquots were extracted using 50 μL capillaries, which were placed in an ultrapure quartz tube and inserted into the cavity of the Bruker EMX CW-micro EPR spectrometer (X-band ~ 9.7 GHz). Experiments were also performed in the presence of 20 mM HMF to observe the influence of this substrate. Furthermore, the detection of DMPO-HMF spin adduce was done in the absence of oxygen (bubbling argon in the suspension). Easy spin [3] was used for simulating DMPO spin adducts spectra.

Catalytic stability measurement

For the first run, 40 mg was used in 8 mL HMF (20mM) CH_3CN solution. After reaction, the catalyst was collected by centrifugation at 8000 rpm to avoid loss and washed by water and ethanol several times. The spent catalyst was dried in an oven at 80 °C and reused for the sequent run. For the second run, 10 mg sample was added to 2 mL HMF CH_3CN solution with the same concentration of 20mM, and other cycles were repeated with the same procedure by adding small amount of used sample. The stability of the catalyst was also measured by photocatalytic water splitting by extending the reaction time to 25hours.

Mott-Schottky measurement

The Mott-Schottky measurement was conducted on a Zennium electrochemical (Zahner, Germany) with three electrodes. The working electrode was prepared via a coating method. Briefly, 20 mg sample was dispersed in a mixture of 100 μL Nafion solution (5wt.%) and 900 μL isopropyl alcohol under ultrasonic for 10 min, then the dispersion was dropped on a FTO glass with an active area of 1.5×1.5 cm^2 and dried naturally in air. Pt wire and Ag/AgCl (3M, NaCl) were used as the counter electrode and the reference electrode, respectively. The electrolyte was sodium sulfate (0.5 M). The Mott-Schottky curves were recorded by electrochemical impedance measurements to obtain the flat-band potential of the photocatalyst.

Photocatalytic water splitting reaction

Photocatalytic water splitting experiments were performed in a double jacket three neck flasks, and the gas space in the reactor about the liquid phase was only low. Typically, 25 mg of photocatalyst was dispersed in 50 mL of distilled water in absence of any cocatalyst or sacrificial agent. The reaction was performed at 25 °C. Before the lamp was switched on, the solution was purged with Ar for 30 min to minimize the air in the system. Then, the Ar flow was reduced to a constant flow rate of 2.5 $mL \cdot min^{-1}$. Subsequently, the reactor was exposed under a 300 W Xenon lamp source (LSE341, LOT Quantum Design, wavelength: 300-700nm, light intensity: 1000mW cm^{-2}) equipped with a 90° deflection reflector system (MS 90) containing a dichroic mirror. The evolved gas was analyzed online each 15 min by gas chromatography (GC) using a thermal conductivity detector (TCD). The H_2 evolution rate was determined by using the following equation:

$$r_{H2}(\mu mol \cdot h^{-1}) = \frac{F_{Ar}(mL \cdot min^{-1}) A_{H2}^{GC} * 60000}{f_{H2}^{GC}(1/vol\%) \cdot 100 vol\% \cdot M_v(mL \cdot mmol^{-1})}$$

F_{Ar} is the Ar flow rate, A_{H2} is the GC area of the H_2 peak, f_{H2} is the calibration factor of H_2 (H_2 was determined as vol%), and M_V is the molar volume at 25 °C (24.5 $mL \cdot mmol^{-1}$). Because H_2 evolution affects the Ar gas flow rate only in a very minor degree, the inlet Ar flow rate was used for the calculation of the hydrogen formation rate. Hydrogen formation with time (μmol) was obtained by integrating the hydrogen formation rate over different time periods.

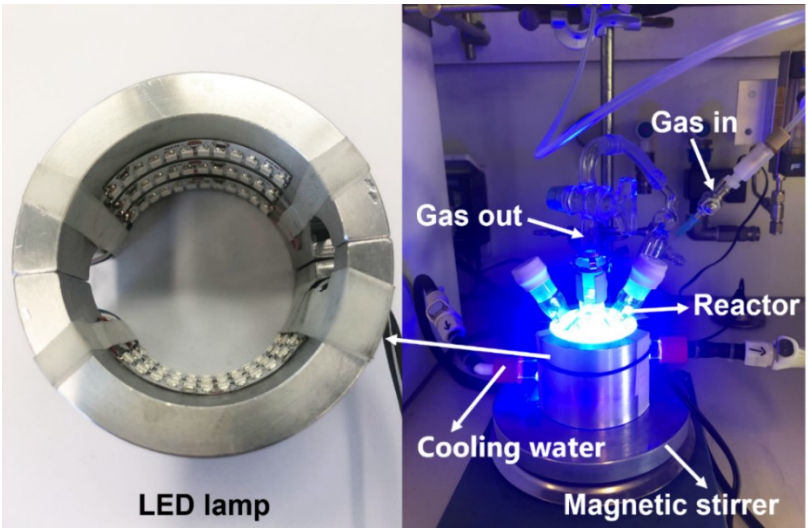

Fig. S1 Experimental set-up used for HMF oxidation (blue LED light intensity:25mW cm^{-2}, maximum wavelength: 467nm).

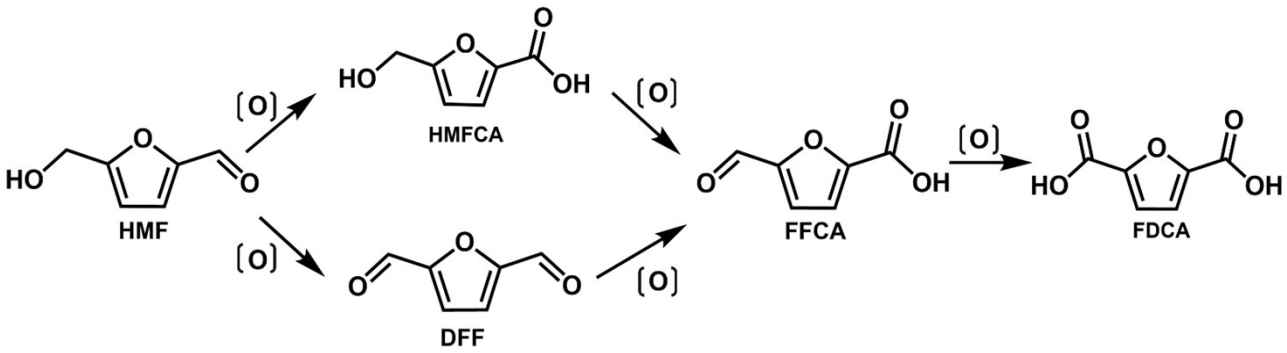

Fig. S2 Schematic illustration of the potential oxidation products from HMF.

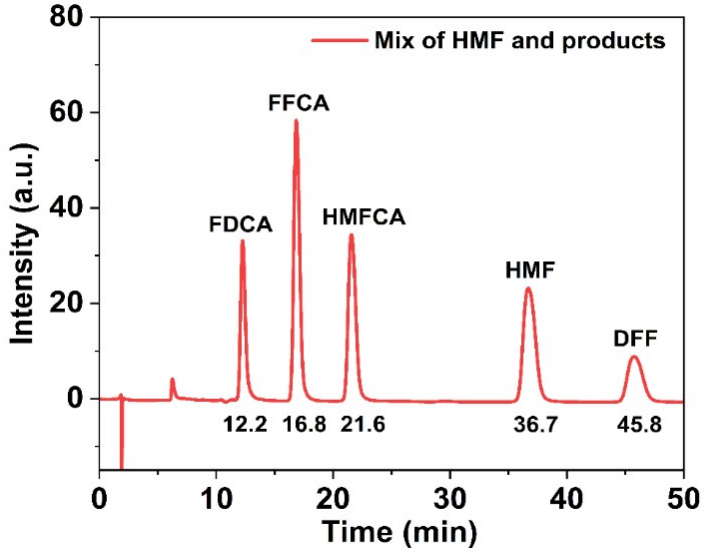

Fig. S3 HPLC chromatogram of the mixture of HMF and possible oxidation products.

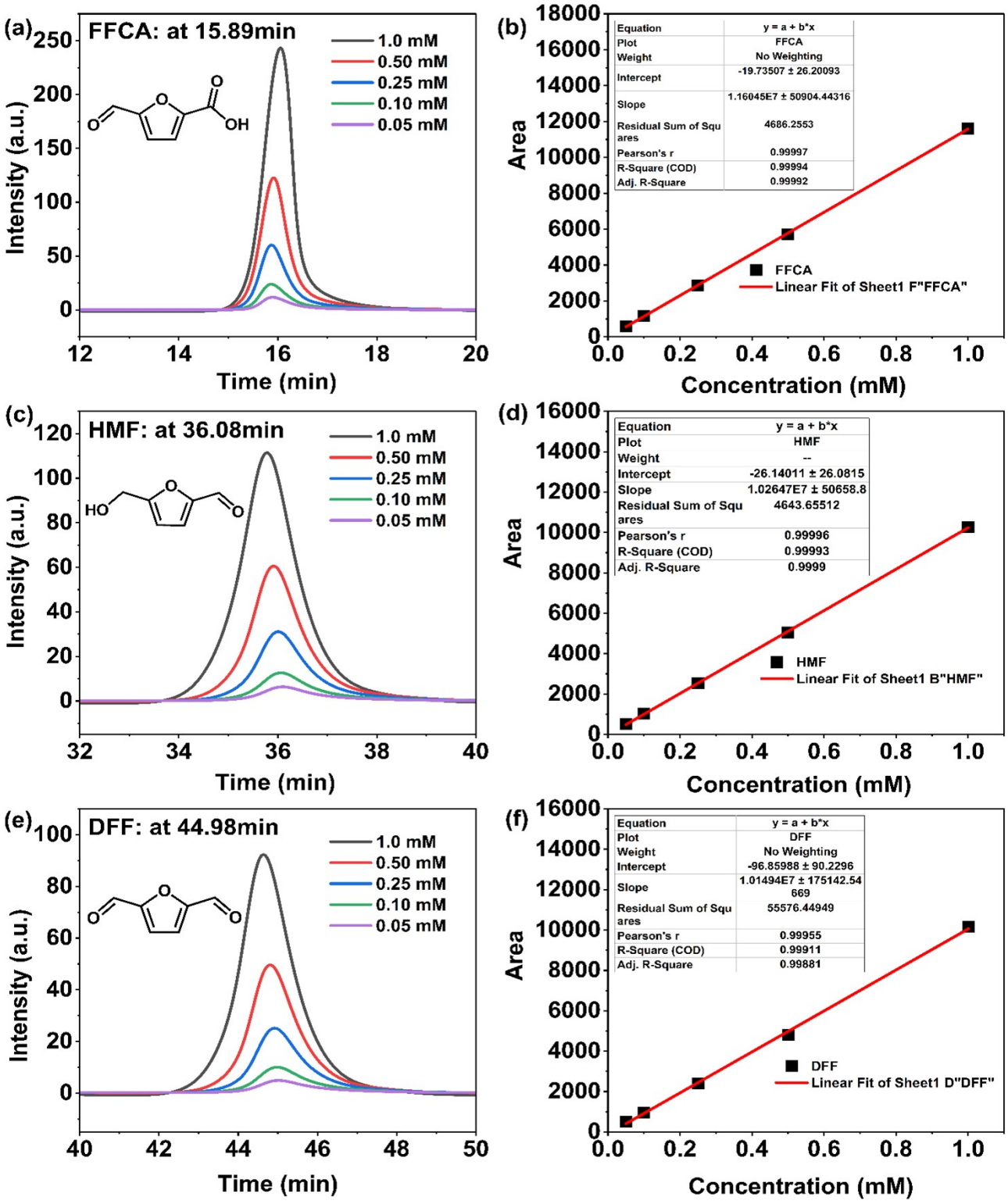

Fig. S4 HPLC chromatograms and calibration curves of FFCA, HMF and DFF.

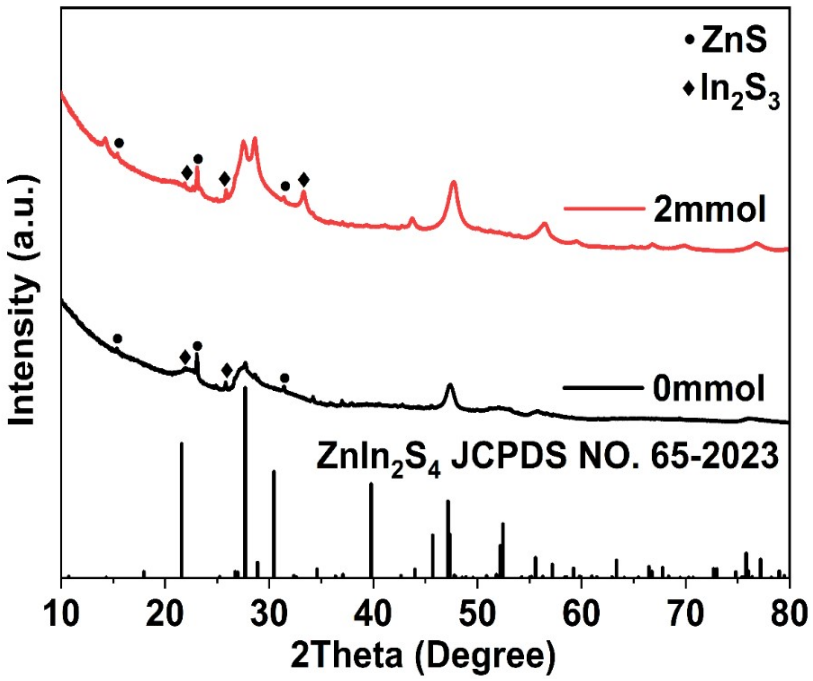

Fig. S5 XRD powder patterns of the sample synthesized without and with 2 mmol trisodium citrate.

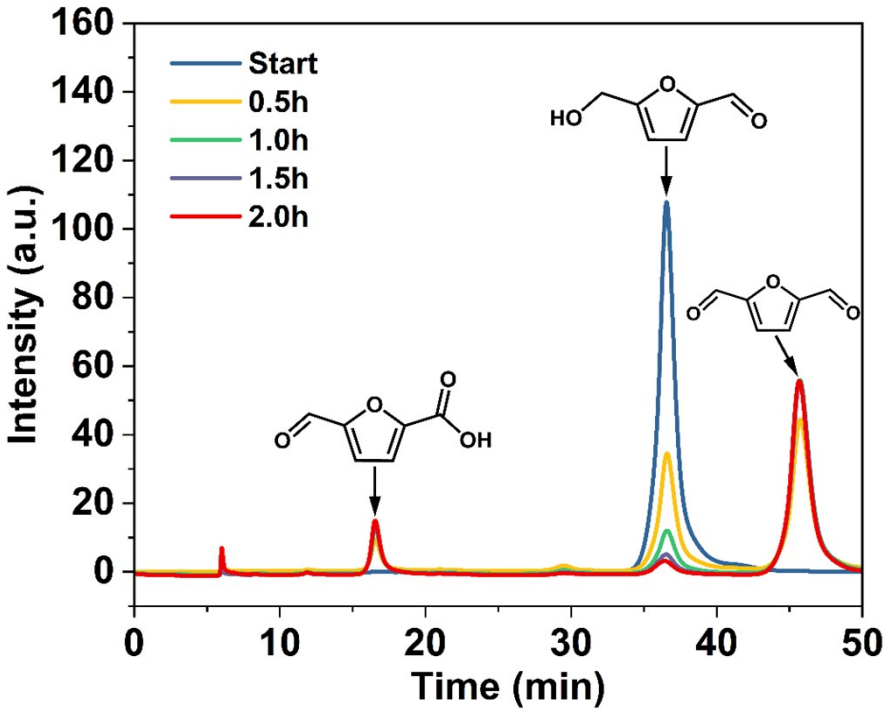

Fig. S6 HPLC chromatogram of reaction mixture during HMF oxidation over $ZnIn_2S_4$. Reaction conditions: 40mg $ZnIn_2S_4$, 20mM HMF, 8mL CH_3CN, 15 °C, air, blue LED.

Table S1 Comparison of photocatalysts for oxidation of HMF to DFF.

Photocatalyst	Light source	Solvent	HMF concentration (mM)	Time (h)	Conv. (%)	DFF Sel. (%)	DFF Yield (%)	Ref.
$ZnIn_2S_4$	Blue LED	MeCN	20.0	1.5	95.0	70.0	66.5	This work
$ZnIn_2S_4$	300W Xe lamp	MeCN	5.0	1	91.1	99.4	90.6	[4]
$MAPbBr_3$	Blue LED	MeCN	5.0	10	100	90 ± 1.2	90 ± 1.2	[5]
P-$Zn_xCd_{1-x}S$	White LED	water	16	8	40	65	26	[6]
$ZnIn_2S_4$/ Nb_2O_5	Simulated solar light	$PhCF_3$	10	3	85.5	88.3	75.5	[7]
SGCN/ Pt	LED (λ>400 nm)	DMF	10.0	48	38.4	>99	38.4	[8]
SGH-TiO_2	Green LED (λ=515 nm)	MeCN	1.0	0.5	59	87	52	[9]
Fe (III)/ Bi_2MoO_6	500 W Xe lamp (λ>400 nm)	water	20	8	32.6	95.3	31.1	[10]
Nb_2O_5-800	Xe lamp (λ>400 nm)	$PhCF_3$	0.1	6	19.2	90.6	17.4	[11]
Water treated g-C_3N_4	Xe lamp (λ>400 nm)	MeCN+ $PhCF_3$	20	6	31.2	85.6	26.7	[12]
WO_3/ g-C_3N_4	Xe lamp (λ>400 nm)	MeCN+ $PhCF_3$	0.1	6	27.4	87.2	23.9	[13]
CTF-Th@SBA-15	Blue LED (λ=460 nm)	water	10	30	57	99	56.4	[14]
$Zn_{0.5}Cd_{0.5}S$/ MnO_2	30W white LED	water	15.9	24	46.6	100	46.6	[15]
CdS	Blue LED	MeCN/$Mn(NO_3)_2$	25	48	99	99	99	[16]

Table S2 Reproducibility of $ZnIn_2S_4$ for photocatalytic HMF oxidation.

Entry	Conv. (%)	DFF Sel. (%)	DFF Yield (%)	FFCA Sel. (%)	FFCA Yield (%)
1	96.1	69.8	67.1	7.2	6.9
2	95.2	67.8	64.6	6.8	6.5
3	95.9	70.6	67.8	5.7	5.5
Average	95.7	69.4	66.5	6.6	6.3

Reaction conditions: 10 mg $ZnIn_2S_4$, 20 mM HMF, 2 mL CH_3CN, 15 °C, air, 2h, blue LED.

Table S3 Photocatalytic conversion of HMF to DFF and FFCA over different photocatalysts.

Entry	Sample	Conv. (%)	DFF Sel. (%)	DFF Yield (%)	FFCA Sel. (%)	FFCA Yield (%)
1	$ZnIn_2S_4$ (with sodium citrate)	95.7	69.4	66.5	6.6	6.3
2	$ZnIn_2S_4$ (without sodium citrate)	47.3	28.9	13.8	3.2	1.5
3	ZnS	4.9	44.0	2.2	0	0
4	In_2S_3	5.3	47.6	2.5	0	0

Reaction conditions: 10 mg photocatalyst, 20 mM HMF, 2 mL CH_3CN, 15 °C, air, 2h, blue LED.

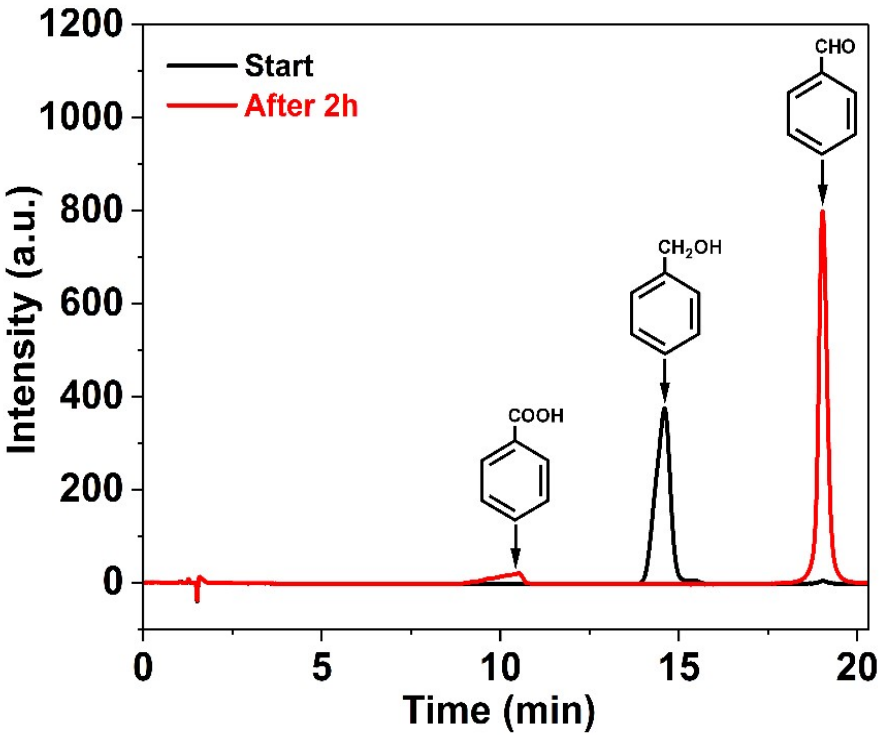

Fig. S7 HPLC chromatogram of reaction mixture of photocatalytic benzyl alcohol oxidation over $ZnIn_2S_4$. Reaction conditions: 10mg $ZnIn_2S_4$, 20mM benzyl alcohol, 2 mL CH_3CN, 15 °C, air, blue LED.

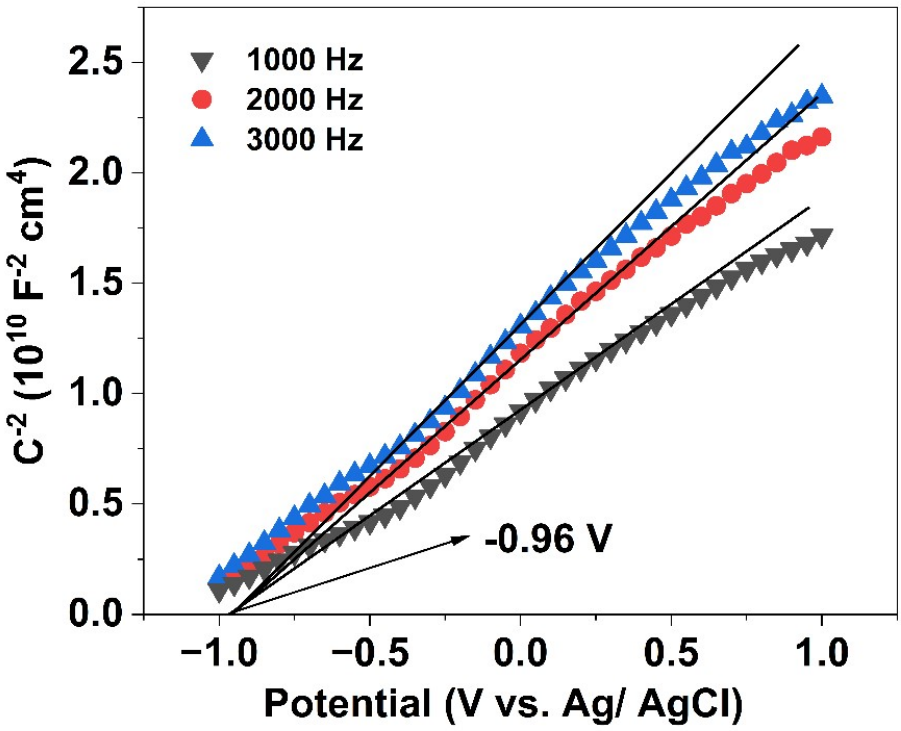

Fig. S8 The Mott-Schottky curve of $ZnIn_2S_4$.

E_{FB} (flat band potential) =-0.96 V

E_{CB} (conduction band minimum) =-1.06 V, E_{CB} is 0.1 V more negative than E_{FB}

E_{CB} (NHE) = E_{CB} + 0.059 pH + $E^{o}_{Ag/AgCl}$

$E^{o}_{Ag/\ AgCl}$=0.209 V

E_{CB} (NHE) = E_{CB} + 0.059 V pH + 0.209 V

E_{CB} (NHE) = -1.06 V+ 0.059 V * 7 + 0.209 V= -0.44 V

E_{VB} (NHE) = E_{CB} (NHE) + E_g (band gap energy, 2.63 eV)

Therefore, the CB (conduction band) minimum and the VB (valence band) maximum potentials of $ZnIn_2S_4$ (pH=0) were calculated to be -0.44 V and +2.19 V, respectively.

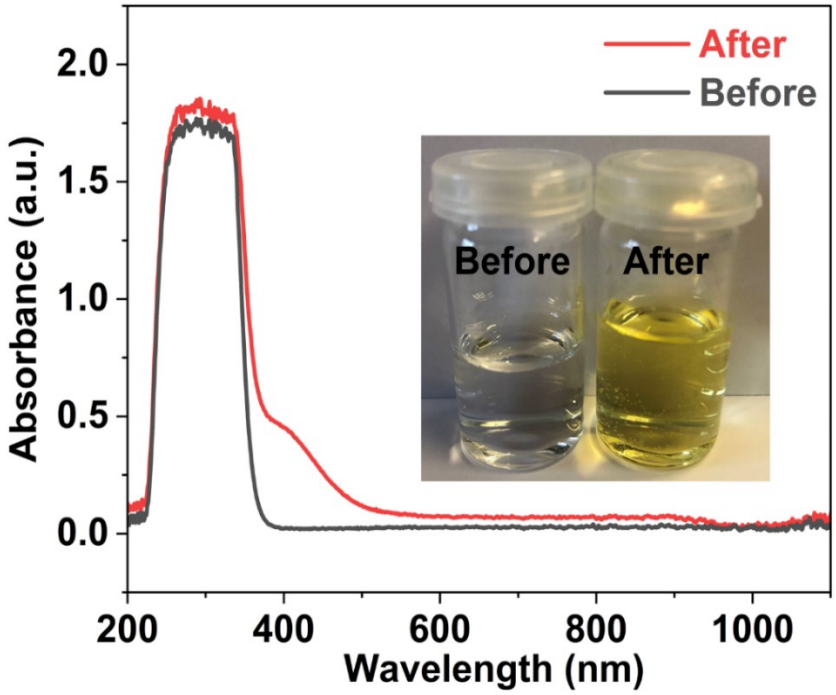

Fig. S9 Uv-vis spectra of the solution after adding ammonium titanyl oxalate monohydrate. Reaction conditions: 10mg $ZnIn_2S_4$, 20mM HMF, 2mL CH_3CN, 15 °C, air, blue LED.

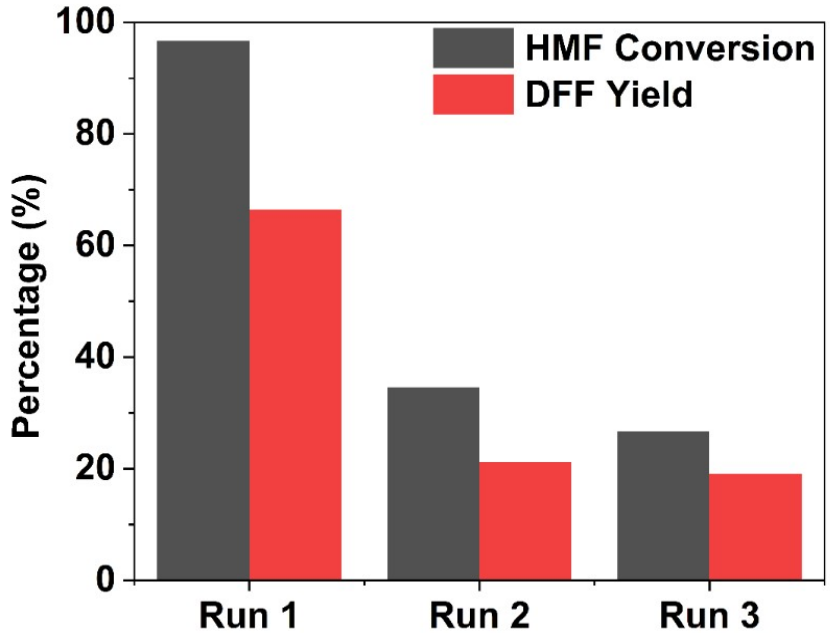

Fig. S10 Photocatalytic HMF oxidation stability meassurement of $ZnIn_2S_4$. Reaction conditions: 10mg $ZnIn_2S_4$, 20mM HMF, 2mL CH_3CN, 15 °C, air, blue LED.

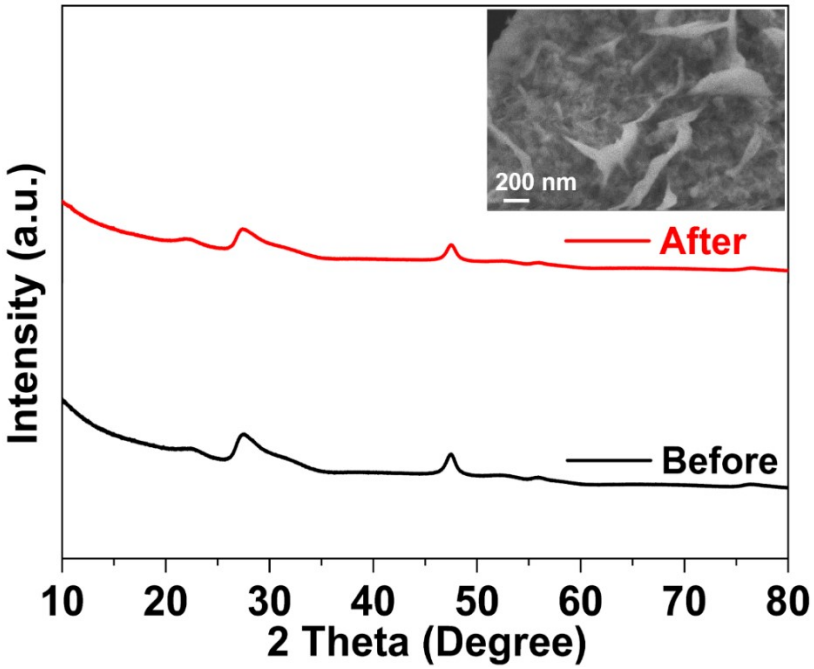

Fig. S11 XRD powder patterns and (b) the corresponding SEM image of $ZnIn_2S_4$ after cycling stability test.

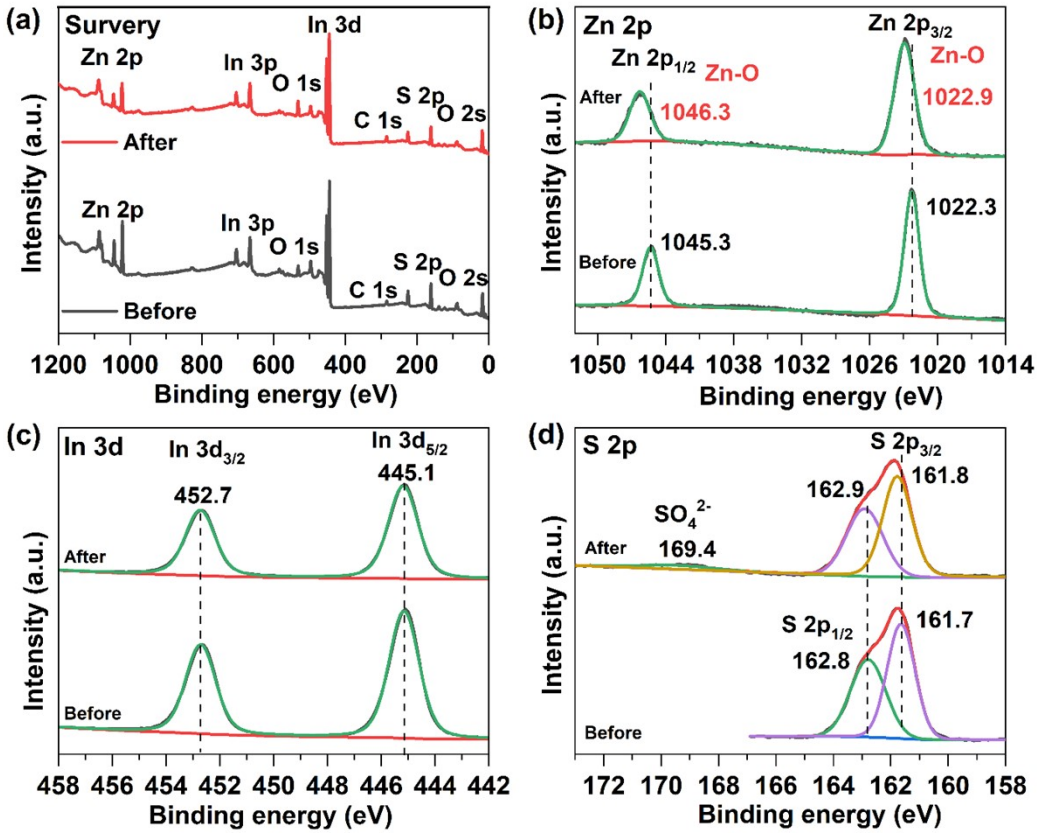

Fig. S12 XP spectra of $ZnIn_2S_4$ before and after cycling experiment: (a) Survey, (b) Zn 2p, (c) In 3d, and (d) S2p.

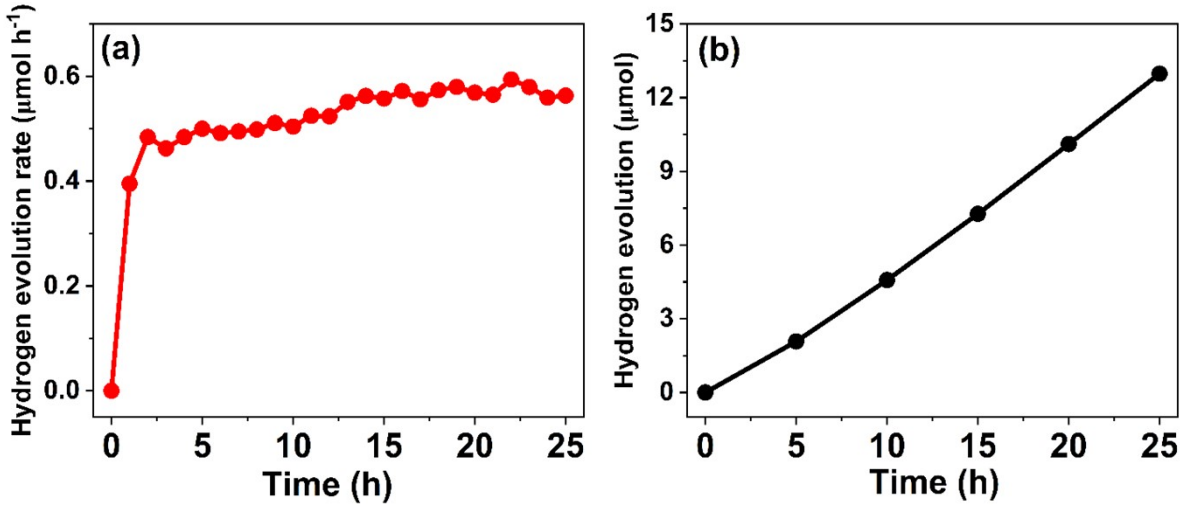

Fig. S13 (a) Photocatalytic H_2 evolution rate of ZIS, and (b) results of a long-term experiment under white light irradiation using ZIS in pure water without co-catalyst and sacrificial agent.

References

1. R. M. Sellers, Analyst, 1980, **105**, 950-954.
2. M. A. da Silva, I. F. Silva, Q. Xue, B. T. Lo, N. V. Tarakina, B. N. Nunes, P. Adler, S. K. Sahoo, D. W. Bahnemann and N. López-Salas, Appl. Catal. B: Environ., 2022, **304**, 120965.
3. S. Stoll and A. Schweiger, J. Magn. Reson., 2006, **178**, 42-55.
4. H. Zhao, D. Trivedi, M. Roostaeinia, X. Yong, J. Chen, P. Kumar, J. Liu, B.-L. Su, S. Larter and M. G. Kibria, Green Chem., 2023, **25**, 692-699.
5. M. Zhang, Z. Li, X. Xin, J. Zhang, Y. Feng and H. Lv, ACS Catal., 2020, **10**, 14793-14800.
6. H.-F. Ye, R. Shi, X. Yang, W.-F. Fu and Y. Chen, Appl. Catal. B: Environ., 2018, **233**, 70-79.
7. Y. Wang, X. Kong, M. Jiang, F. Zhang and X. Lei, Inorg. Chem. Front., 2020, **7**, 437-446.
8. V. R. Battula, A. Jaryal and K. Kailasam, J. Mater. Chem. A, 2019, **7**, 5643-5649.
9. A. Khan, M. Goepel, A. Kubas, D. Łomot, W. Lisowski, D. Lisovytskiy, A. Nowicka, J. C. Colmenares and R. Gläser, ChemSusChem, 2021, **14**, 1351-1362.
10. J. Xue, C. Huang, Y. Zong, J. Gu, M. Wang and S. Ma, Appl. Organomet. Chem., 2019, **33**, e5187.
11. H. Zhang, Q. Wu, C. Guo, Y. Wu and T. Wu, ACS Sustain. Chem. Eng., 2017, **5**, 3517-3523.
12. Q. Wu, Y. He, H. Zhang, Z. Feng, Y. Wu and T. Wu, Mol. Catal., 2017, **436**, 10-18.
13. H. Zhang, Z. Feng, Y. Zhu, Y. Wu and T. Wu, J. Photochem. Photobiol. A, 2019, **371**, 1-9.
14. C. Ayed, W. Huang, G. Kizilsavas, K. Landfester and K. A. Zhang, ChemPhotoChem, 2020, **4**, 571-576.
15. S. Dhingra, T. Chhabra, V. Krishnan and C. Nagaraja, ACS Appl. Energy Mater., 2020, **3**, 7138-7148.
16. J. L. DiMeglio, A. G. Breuhaus-Alvarez, S. Li and B. M. Bartlett, ACS Catal., 2019, **9**, 5732-5741.